

# The optical potential of ${}^6\text{He}$ in the eikonal approximation

B. Abu-Ibrahim<sup>1,2</sup> and Y. Suzuki<sup>1</sup>

<sup>1</sup> Department of Physics, Niigata University, Niigata 950-2181, Japan

<sup>2</sup> Department of Physics, Cairo University, Giza 12613, Egypt

(November 1, 2018)

## Abstract

The new data of the elastic scattering of  ${}^6\text{He}+{}^{12}\text{C}$  at about 40 MeV/nucleon are analyzed in the eikonal approximation. The  ${}^6\text{He}+{}^{12}\text{C}$  phase-shift function is evaluated completely without any *ad hoc* assumption by a Monte Carlo integration, which makes it possible to use a realistic 6-nucleon wave function for a halo nucleus  ${}^6\text{He}$ . The effect of the breakup of  ${}^6\text{He}$  on the elastic differential cross sections as well as the optical potential is studied at different energies from 40 to 800 MeV/nucleon.

PACS number(s): 24.10.-i; 21.60.Ka; 25.60.Bx; 25.10.+s

Keywords: Eikonal; Glauber; Monte Carlo; Halo; Breakup

## I. INTRODUCTION

A measurement of elastic scatterings of a projectile nucleus by a target nucleus provides unique information on the nuclear density distribution as well as the optical potential between them. The measurements of the angular distribution of purely elastic scattering for unstable nuclei are, however, very few so far because the separation of elastic and inelastic scatterings is in general difficult. Very recently the elastic scattering of  ${}^6\text{He}$  on  ${}^{12}\text{C}$  has been measured at 38.3 MeV/nucleon up to about 20° in the center-of-mass (c.m.) frame [1], which covers considerably wider angles than the previous measurement at 41.6 MeV/nucleon [2]. The new data will give us better opportunity to study the interaction potential between  ${}^6\text{He}$  and  ${}^{12}\text{C}$ .

The nucleus  ${}^6\text{He}$  has attracted much experimental and theoretical interest as a two-neutron halo nucleus: It breaks to  ${}^4\text{He}+n+n$  by the small energy input of 0.975 MeV. It is Borromean as the three-body system of  ${}^4\text{He}+n+n$ . At the present stage of experimental precision, the  $\alpha+n+n$  model appears to be entirely satisfactory [3]. More sophisticated approach may be called for in some cases. For example, the breaking up of the  $\alpha$ -cluster is necessary to deeply understand the binding mechanism of  ${}^6\text{He}$  [4].

The weak binding of a halo nucleus implies that it can easily decay to its constituents. Its ground state, lying close to the decay threshold, has a strong coupling to continuum states or resonances during the interaction with a target. This requires a special treatment of the coupling effect on the interaction potential for the halo projectile.

A folding potential derived from an appropriate effective nuclear force, combined with a phenomenological imaginary term, has been successful for describing the elastic scattering

of various systems [5]. A substantial reduction of the real strength of the folding potential has, however, been found necessary for weakly bound projectiles like  $^{6,7}\text{Li}$  and  $^9\text{Be}$  [5,6]. This effect is explained by coupled-channel calculations in which projectile excitations are explicitly taken into account. The excitation of a weakly bound projectile into the continuum states has an important influence on the elastic scattering, and in the optical model this has to be mocked up by a substantial reduction of the depth of the real potential term. The difference from the folding potential is called a dynamic polarization potential.

Since a halo nucleus is an extreme case of a weakly bound projectile, a similar effect is expected for halo-nucleus projectiles, thus the applicability of the folding model to halo nuclei is questionable. In fact, the double-folding model using a realistic density-dependent nucleon-nucleon (NN) interaction, combined with the imaginary part taken in the conventional Woods-Saxon form, fails to reproduce the measured  $^6\text{He} + ^{12}\text{C}$  elastic differential cross sections over the whole angular range [1].

The inclusion of continuum states is performed by a continuum-discretized coupled-channel method, in which the continuum states of the projectile are approximated by a set of discrete states and each of them couples with the relative motion between the projectile and the target. For the two-neutron halo nucleus  $^6\text{He}$  the continuum states are three-body states, so in the continuum-discretized coupled-channel approach to the  $^6\text{He} + ^{12}\text{C}$  scattering one must solve a four-body Schrödinger equation, which, even if possible, will become very computer-time consuming. It is certainly impossible at present if one wants to consider the effect of, e.g., the distortion of the  $\alpha$ -core.

A way out to overcome this difficulty is to use the eikonal approximation for composite-particle scattering [7–10], which is known as the Glauber theory [11] when all the constituents of the colliding nuclei are treated on an equal footing. We will show that a full Glauber calculation does not necessarily reproduce the new elastic scattering data but an effective phase calculated from a nucleon-target (NT) optical potential instead improves the description of the scattering. The utility of the approach has been tested even at low energies around 100 MeV/nucleon [12]. With the use of the eikonal approximation it is straightforward to obtain the dynamic polarization potential. The purpose of this paper is to show that the new  $^6\text{He} + ^{12}\text{C}$  data can substantially be understood in the eikonal approximation without introducing any *ad hoc* assumptions and in addition to study the energy dependence of the optical potential of the  $^6\text{He} + ^{12}\text{C}$  system. We stress the characteristic points and the strength of the present approach: Firstly, a nucleon- $^{12}\text{C}$  optical potential is used as a basic input of our calculation. Secondly,  $^6\text{He}$  is described with a realistic (6-nucleon) wave function which is obtained by variational Monte Carlo (VMC) calculation [13]. By this the calculation of Ref. [12] is further extended to directly use the wave function itself of  $^6\text{He}$  (but not just the density). Thirdly, the scattering amplitude is calculated with the help of a Monte Carlo integration to all orders in the eikonal approximation.

In sect. II the scattering amplitude for composite-particle scatterings is briefly introduced in the eikonal approximation. In sect. III an effective phase-shift function is defined by considering a target nucleus as a scatterer. The  $^6\text{He} + ^{12}\text{C}$  elastic scattering at 40 MeV/nucleon is analyzed and the optical potential including the breakup of  $^6\text{He}$  is derived using the phase-shift function. In sect. IV the energy dependence of the dynamic polarization potential is studied. A summary is given in sect. V.

## II. EIKONAL APPROXIMATION FOR COMPOSITE-PARTICLE SCATTERING

For a scattering problem of composite particles, the exact calculation of the scattering amplitude is extremely difficult. Appropriate approximations are indispensable. When the incident energy is high or the incident wave number  $K$  is large enough, the relative motion between the projectile and the target oscillates rapidly and its deviation from a plane wave is expected to be small. This leads to the eikonal approximation. The applicability of the eikonal approximation may be tested by a comparison to a fully quantum-mechanical calculation for a simple potential scattering problem. For this aim we take a single-folding potential for elastic scatterings of  ${}^6\text{He}$  on  ${}^{12}\text{C}$  at 40 MeV/nucleon. (The detail of this potential will be explained later.) It is found that the elastic differential cross section calculated in the eikonal approximation is by at most 15% larger than the exact one up to  $30^\circ$  excepting around the cross section minimum. The discrepancy grows to about five times at  $60^\circ$ . Thus the eikonal approximation works reasonably well for angles smaller than  $30^\circ$  at this energy. See also Ref. [14] for the study of the accuracy of the eikonal calculations.

A further approximation called an adiabatic approximation is needed to derive a simple, tractable expression for the scattering amplitude. In this approximation the excitation energies of the colliding nuclei are neglected. Under these approximations the scattering amplitude is given by

$$f_{\alpha\beta}(\theta, \phi) = \frac{iK}{2\pi} \int d\mathbf{b} e^{-i\mathbf{q}\cdot\mathbf{b}} \langle \psi_{\alpha}^{(\text{P})} \psi_{\beta}^{(\text{T})} | 1 - e^{i \sum_{i \in \text{P}} \sum_{j \in \text{T}} \chi_{\text{NN}}(\mathbf{b} + \mathbf{s}_i^{(\text{P})} - \mathbf{s}_j^{(\text{T})})} | \psi_0^{(\text{P})} \psi_0^{(\text{T})} \rangle, \quad (1)$$

where  $\mathbf{q}$  is the momentum transferred from the target to the projectile,  $\mathbf{b}$  a two-dimensional impact-parameter vector perpendicular to the  $z$ -direction, and e.g.,  $\mathbf{s}_i^{(\text{P})}$  is the projection onto the  $xy$ -plane of the nucleon position vector relative to the projectile's c.m.,  $\mathbf{r}_i^{(\text{P})} - \mathbf{R}_{\text{c.m.}}^{(\text{P})}$ . The wave function  $\psi_{\alpha}^{(\text{P})}$  denotes the projectile's intrinsic state specified by a quantum number  $\alpha$  with its c.m. part being dropped. ( $\alpha = 0$  stands for the ground state.) Similarly the target state is denoted  $\psi_{\beta}^{(\text{T})}$ . Thus  $f_{00}$  stands for the elastic scattering amplitude. See, for example, Refs. [11,3] for more details.

The phase-shift function  $\chi_{\text{NN}}$  in Eq. (1) is a basic ingredient for the scattering amplitude. It describes the NN scattering and is related to the NN potential  $V_{\text{NN}}$  by

$$\chi_{\text{NN}}(\mathbf{b}) = -\frac{1}{\hbar v} \int_{-\infty}^{+\infty} dz V_{\text{NN}}(\mathbf{b} + z\hat{\mathbf{z}}), \quad (2)$$

where  $v$  is the asymptotic velocity of the relative motion between the projectile and the target and  $\hat{\mathbf{z}}$  is a unit vector in the  $z$ -direction. The NN potential contains complicated spin-isospin dependence, so  $\chi_{\text{NN}}$  in general becomes an operator acting in that space. The use of such an operator in Eq. (1) is extremely involved, and here it is treated as just a function by ignoring the spin-isospin dependence as is usually done. However, we distinguish protons and neutrons when necessary. The NN profile function  $\Gamma_{\text{NN}}(\mathbf{b})$  is introduced and often parametrized in the form

$$\begin{aligned} \Gamma_{\text{NN}}(\mathbf{b}) &= 1 - e^{i\chi_{\text{NN}}(\mathbf{b})} \\ &= \frac{1 - i\alpha}{2\pi} \omega \sigma_{\text{NN}} e^{-\omega \mathbf{b}^2}. \end{aligned} \quad (3)$$

Here  $\sigma_{\text{NN}}$  is the total NN cross section and the parameters  $\alpha$  and  $\omega$  are determined so as to fit the NN elastic differential cross section as well as the NN reaction cross section at relevant energy.

To get the elastic scattering amplitude  $f_{00}$  we need to calculate the phase-shift function  $\chi(\mathbf{b})$ :

$$e^{i\chi(\mathbf{b})} = \langle \psi_0^{(\text{P})} \psi_0^{(\text{T})} | \prod_{i \in \text{P}} \prod_{j \in \text{T}} [1 - \Gamma_{\text{NN}}(\mathbf{b} + \mathbf{s}_i^{(\text{P})} - \mathbf{s}_j^{(\text{T})})] | \psi_0^{(\text{P})} \psi_0^{(\text{T})} \rangle. \quad (4)$$

The above matrix element contains a multi-dimensional integration, which is obviously not easy to perform in general. Recently it has been demonstrated [15] that the phase-shift function can be evaluated by Monte Carlo method without approximation. The effectiveness of the method has been illustrated by several examples and will be used in this study as well.

First we ask how well the Glauber model reproduces the elastic scattering data on  ${}^6\text{He} + {}^{12}\text{C}$ . The wave function used for  ${}^6\text{He}$  is the variational Monte Carlo (VMC) wave function [13]. The VMC method starts with the construction of a variational trial function of specified angular momentum, parity and isospin, using products of two- and three-body correlation operators acting on a fully antisymmetrized set of one-body basis states. This wave function is obtained by minimizing the energy of the nuclear Hamiltonian which includes realistic two- (Argonne  $v_{18}$  [16]) and three-body (Illinois IL2 [17]) interactions. The root mean square (r.m.s.) radii with the VMC wave function are 2.56, 1.96 and 2.81 fm for nucleon, proton and neutron, respectively. The  ${}^{12}\text{C}$  nucleus is not yet accessible in a realistic calculation and for the  ${}^{12}\text{C}$  a three- $\alpha$  microscopic cluster-model wave function is used: It gives the r.m.s. radius of 2.36 fm. In this model the intrinsic wave function of the  $\alpha$ -particles is a single shell-model Slater determinant and the relative motion between the clusters is expressed in terms of linear combinations of Gaussians. The combination coefficients are determined variationally by solving the 12-nucleon Schrödinger equation with an effective (Minnesota [18]) two-nucleon interaction. Values of  $\sigma_{\text{NN}}$  and  $\alpha$  defining  $\Gamma_{\text{NN}}$  are taken from literatures and the range parameter  $\omega$  is determined by

$$\frac{1}{\omega} = \frac{1 + \alpha^2}{8\pi} \sigma_{\text{NN}}, \quad (5)$$

which comes out from the condition that the NN total cross section be equal to the NN total elastic cross section. Results of calculation are shown in Fig. 1: Dotted line is obtained by using  $\sigma_{\text{NN}} = 13.5 \text{ fm}^2$  and  $\alpha = 0.9$  [19], while in dashed line different profile functions are used for np and pp (also nn) pairs, i.e.,  $\sigma_{\text{np}} = 21.8 \text{ fm}^2$ ,  $\alpha_{\text{np}} = 0.493$ ,  $\sigma_{\text{pp}} = 7 \text{ fm}^2$ ,  $\alpha_{\text{pp}} = 1.328$  [20]. Both calculations give similar cross sections up to  $14^\circ$  and show some difference around the third and fourth minima. An interesting point is that the Glauber model reproduces the data only up to  $7^\circ$  and beyond this angle gives much smaller cross sections than the measurement. Apparently this discrepancy indicates that at 40 MeV/nucleon multiple scatterings occurring in the composite-particle scattering are not quite well represented by the NN scattering determined in free space but receives some modifications by medium effects.

Though it does not reproduce the data well except for small angles, the Glauber model can include breakup effects of the projectile and the target. Before going to the next section,

we attempt to assess the importance of the breakup effect of  ${}^6\text{He}$  in the elastic scattering. For this purpose we show in Fig. 1 the differential cross sections (solid line) calculated fully quantum-mechanically with the single-folding potential  $U_f(R)$

$$U_f(R) = \int d\mathbf{r} \rho^{(P)}(\mathbf{r}) V_{\text{NT}}(\mathbf{R} + \mathbf{r}) \quad (6)$$

with the projectile density

$$\rho^{(P)}(\mathbf{r}) = \langle \psi_0^{(P)} | \sum_{i \in P} \delta(\mathbf{r}_i^{(P)} - \mathbf{R}_{\text{c.m.}} - \mathbf{r}) | \psi_0^{(P)} \rangle, \quad (7)$$

where  $\mathbf{R}$  is the distance vector between the projectile and the target and  $V_{\text{NT}}$  is an NT optical potential. This single-folding model gives both real and imaginary potentials automatically. The folding model is found to overestimate the measured cross sections beyond  $6^\circ$ , which is in contrast to the full Glauber-model calculation. It also cannot reproduce simultaneously the first deep minimum and the third maximum as noted in Ref. [1], where the double-folding model is used to generate the  ${}^6\text{He}-{}^{12}\text{C}$  potential and the imaginary part was adjusted to fit the data. The overestimation of the single-folding model is due to neglecting the breakup effect of  ${}^6\text{He}$ . This will be discussed later in more detail.

### III. EFFECTIVE EIKONAL PHASE

In the previous section we have observed that the Glauber model with the NN profile function does not necessarily reproduce the data. Since the NN profile function is chosen to be consistent with the data of the elementary NN scattering in free space, this suggests that an appropriate effective interaction has to be employed in the calculation. Instead of using such an effective interaction like  $G$ -matrix, we proposed a simple, practical approach [21,12] to composite-particle scatterings by considering the target just a scatterer and taking an NT scattering as an elementary vehicle.

In this formalism various effects such as the Fermi motion and the Pauli-blocking, etc., would be included to some extent through the NT amplitude determined from an NT optical potential. The effective optical phase-shift function is thus given by

$$\begin{aligned} e^{i\tilde{\chi}(\mathbf{b})} &= \langle \psi_0^{(P)} | e^{i \sum_{i \in P} \chi_{\text{NT}}(\mathbf{b} + \mathbf{s}_i^{(P)})} | \psi_0^{(P)} \rangle \\ &= \langle \psi_0^{(P)} | \prod_{i \in P} \left[ 1 - \Gamma_{\text{NT}}(\mathbf{b} + \mathbf{s}_i^{(P)}) \right] | \psi_0^{(P)} \rangle, \end{aligned} \quad (8)$$

where  $\Gamma_{\text{NT}} = 1 - e^{i\chi_{\text{NT}}}$  is related to  $V_{\text{NT}}$  through

$$\chi_{\text{NT}}(\mathbf{b}) = -\frac{1}{\hbar v} \int_{-\infty}^{\infty} dz V_{\text{NT}}(\mathbf{b} + z\hat{\mathbf{z}}). \quad (9)$$

The examples of calculation shown in Ref. [21] were obtained by approximating Eq. (8) by

$$e^{i\tilde{\chi}_{\text{OLA}}(\mathbf{b})} = \exp \left\{ - \int d\mathbf{r} \rho^{(P)}(\mathbf{r}) \Gamma_{\text{NT}}(\mathbf{b} + \mathbf{s}) \right\}, \quad (10)$$

where  $\mathbf{s}$  is the projection of  $\mathbf{r}$  onto the  $xy$ -plane. In the present study we will not use this approximation but perform a virtually exact phase-shift calculation by a Monte Carlo method in which  $|\psi_0^{(P)}|^2$  serves as a weight function for sampling configuration points.

It should be noted that the phase-shift function corresponding to the single-folding potential appears as the first term of a cumulant expansion of Eq. (8). To see this we note that the phase-shift function  $\chi_f(\mathbf{b})$  corresponding to  $U_f(R)$  is given by

$$\begin{aligned}\chi_f(\mathbf{b}) &= -\frac{1}{\hbar v} \int_{-\infty}^{\infty} dz U_f(\mathbf{b} + z\hat{\mathbf{z}}) \\ &= \int d\mathbf{r} \rho^{(P)}(\mathbf{r}) \chi_{NT}(\mathbf{b} + \mathbf{s}) \\ &= \langle \psi_0^{(P)} | \sum_{i \in P} \chi_{NT}(\mathbf{b} + \mathbf{s}_i^{(P)}) | \psi_0^{(P)} \rangle.\end{aligned}\quad (11)$$

By substituting Eq. (11) into Eq. (8), we obtain the following expression

$$e^{i\tilde{\chi}(\mathbf{b})} = e^{i\chi_f(\mathbf{b})} \langle \psi_0^{(P)} | e^{i\delta\chi} | \psi_0^{(P)} \rangle \quad (12)$$

with

$$\delta\chi = \sum_{i \in P} \chi_{NT}(\mathbf{b} + \mathbf{s}_i^{(P)}) - \chi_f(\mathbf{b}), \quad (13)$$

which will be exploited when we discuss the dynamic polarization potential in sect. IV.

We first consider  ${}^4\text{He} + {}^{12}\text{C}$  elastic scattering at 40 MeV/nucleon. The study of this system will give us information on the  ${}^6\text{He} + {}^{12}\text{C}$  elastic scattering. The  ${}^4\text{He} + {}^{12}\text{C}$  phase-shift function  $\tilde{\chi}$  is calculated by using the VMC wave function for  ${}^4\text{He}$  and three different p- ${}^{12}\text{C}$  optical potentials taken from Refs. [22–24]. The spin-orbit component of the optical potential is ignored in the calculation. All of the optical potentials reproduce reasonably well the p- ${}^{12}\text{C}$  elastic scattering data [25] up to about  $50^\circ$ , but show some deviation from the experimental data beyond that angle. The p- ${}^{12}\text{C}$  and  ${}^6\text{He} + {}^{12}\text{C}$  reaction cross sections calculated by these potentials are listed in Table I. All the potentials have a similar real part except that Fannon *et al.* potential (the set of  $V_0 = -47.2$  MeV) is shorter-ranged and has deeper central strength than the others. For the imaginary part Fannon *et al.* potential is deeper than the others near the surface. A comparison with experiment [26] for  ${}^4\text{He} + {}^{12}\text{C}$  scattering is shown in Fig. 2. The potential of Ref. [22] (solid line) reproduces the data quite well up to  $15^\circ$  and slightly underestimates the cross sections at larger angles, while the other potentials (dashed and dash-dotted lines) overestimate the cross section at the minimum around  $10^\circ$ . To see the sensitivity of the cross section to wave functions, we repeated the calculation by using the single harmonic-oscillator shell-model wave function for  ${}^4\text{He}$  with its c.m. part being dropped. The oscillator parameter was set to reproduce the same r.m.s. radius as that of the VMC wave function (1.46 fm). The deviation from the VMC case was very small at this energy. As shown in Ref. [15], different predictions of simple model and realistic wave functions can be seen in cross sections corresponding to much higher momentum transfer.

One of the advantages of the present approach is that we rigorously took account of the c.m. problem, thus using the intrinsic coordinate  $\mathbf{s}_i^{(P)}$  measured from the c.m. of the

projectile. Several authors discussed the effect of the c.m. correlation when one calculates the Glauber amplitude [28,29]. Dotted line in Fig. 2 indicates the cross section calculated with the same shell-model wave function but replacing  $\mathbf{s}_i^{(P)}$  with the projection of  $\mathbf{r}_i^{(P)}$  itself onto the  $xy$ -plane. Ignoring the c.m. correlation is found to cause a significant error for such a light nucleus as  $^4\text{He}$ .

The  $^6\text{He} + ^{12}\text{C}$  phase-shift function  $\tilde{\chi}$  is calculated by using the VMC wave function for  $^6\text{He}$ . The cross sections calculated with the three p- $^{12}\text{C}$  optical potentials are displayed in Fig. 3. Rapaport potential (solid line) and Becchetti and Greenlees potential (dashed line) appear to give a fair agreement with the experimental data though at angles less than  $10^\circ$  Fannon *et al.* potential (dotted line) better fits the data. The difference in the cross sections is mainly due to that of the imaginary part of the p- $^{12}\text{C}$  potential. Though all the potentials give similar results of both the elastic differential cross section and the reaction cross section for p- $^{12}\text{C}$ , the  $^6\text{He} + ^{12}\text{C}$  cross sections are different beyond the second minimum. Solid lines in Figs. 1 and 3 employ the same p- $^{12}\text{C}$  optical potential [24]. The difference is that the former is the folding-model calculation, while the latter is the eikonal calculation. The overestimation of the cross sections observed in the folding-model calculation is certainly improved by the eikonal calculation.

The local, energy-dependent, optical potential for the projectile-target scattering can be constructed from the phase-shift function by [11]

$$U(R) = \frac{\hbar v}{\pi} \frac{1}{R} \frac{d}{dR} \int_R^\infty db b \frac{\tilde{\chi}(b)}{\sqrt{b^2 - R^2}}. \quad (14)$$

Once the potential  $U(R)$  is constructed, we can solve a standard radial Schrödinger equation with  $U(R)$  to obtain the exact partial-wave phase shift  $\delta_l$ . Provided the eikonal approximation is valid, we have

$$\tilde{\chi}(b) \approx 2\delta_l, \quad bK = l + \frac{1}{2}. \quad (15)$$

Figure 4 shows the elastic differential cross sections calculated with  $\delta_l$ . The differential cross sections in Figs. 3 and 4 are thus calculated with the same optical potential  $U(R)$ . The difference is that the eikonal approximation is used in Fig. 3, whereas a partial-wave expansion for the scattering amplitude is used in Fig. 4. As was mentioned in the beginning of sect. II, the eikonal approximation is found to slightly overestimate the differential cross section compared to the exact value.

The difference between  $U(R)$  and the single-folding potential  $U_f(R)$  is nothing but the dynamic polarization potential in the eikonal approximation:

$$U_{\text{DPP}}(R) = U(R) - U_f(R). \quad (16)$$

If the  $^6\text{He}$  wave function is factorized as a three-body wave function  $\psi_{\text{FB}}$  consisting of the  $\alpha$ -core and two-neutron parts, the effective phase-shift function of Eq. (8) may be approximated as follows:

$$e^{i\chi_{\text{FB}}(\mathbf{b})} = \langle \psi_{\text{FB}} | [1 - \Gamma_{\text{CT}}(\mathbf{b} + \mathbf{s}_C)] \prod_{i=1,2} [1 - \Gamma_{\text{NT}}(\mathbf{b} + \mathbf{s}_i)] | \psi_{\text{FB}} \rangle, \quad (17)$$

where  $\mathbf{s}_C$  is the projection onto the  $xy$ -plane of the core-c.m. position vector measured from the c.m. and the core-target profile function  $\Gamma_{CT}(\mathbf{b})$  is calculated from an  $\alpha$ - $^{12}\text{C}$  optical potential. This approximation is sometimes called a few-body Glauber model. It is to be noted that even though the  $\alpha+n+n$  model for  $^6\text{He}$  is satisfactory the factorization of the 6-nucleon wave function of  $^6\text{He}$  cannot in general be performed rigorously. Figure 5 displays the differential cross section calculated with a three-body wave function where two-neutron halo wave function is generated from  $0p_{1/2}$  orbit [30]. The  $\alpha$ - $^{12}\text{C}$  optical potential is taken from Ref. [26]. The cross section calculated by the few-body Glauber model is as good as that of the eikonal calculation using the 6-nucleon wave function (compare to Fig. 3). However, it is found that the different  $p$ - $^{12}\text{C}$  optical potentials lead to only a small difference in the cross section in the case of the few-body Glauber model, which is in contrast to the 6-nucleon calculation. This is probably because the  $\alpha$ - $^{12}\text{C}$  interaction dominates the whole phase-shift responsible for the scattering process. It seems that the approach based on the 6-nucleon eikonal calculation is more natural than the few-body approach particularly when we discuss the energy dependence of the optical potential for  $^6\text{He}$ .

#### IV. DYNAMIC POLARIZATION POTENTIAL OF $^6\text{HE}$

From Eq. (12) we have the following relation

$$\begin{aligned}\tilde{\chi}(\mathbf{b}) &= \chi_f(\mathbf{b}) - i \ln \langle \psi_0^{(P)} | e^{i\delta\chi} | \psi_0^{(P)} \rangle \\ &= \chi_f(\mathbf{b}) + \frac{i}{2} \langle (\delta\chi)^2 \rangle - \frac{1}{6} \langle (\delta\chi)^3 \rangle - \frac{i}{24} \langle (\delta\chi)^4 \rangle + \frac{i}{8} \langle (\delta\chi)^2 \rangle^2 + \dots\end{aligned}\quad (18)$$

Here e.g.,  $\langle (\delta\chi)^2 \rangle = \langle \psi_0^{(P)} | (\delta\chi)^2 | \psi_0^{(P)} \rangle$  and use is made of the property  $\langle \delta\chi \rangle = 0$ . Substituting this cumulant expansion to Eq. (14) we have the corresponding decomposition of the optical potential, and the first term in the expansion is nothing but the folding potential  $U_f$ . Thus the dynamic polarization potential is contributed by those potentials that correspond to the terms  $\langle (\delta\chi)^n \rangle$  ( $n = 2, 3, \dots$ ) arising from the breakup of the projectile.

One can predict the sign of the dynamic polarization potential under certain conditions [7,3]. Assuming that the  $V_{NT}$  has the form  $V_{NT}(R) \sim (V_0 + iW_0)f(R)$ , the sign of the term  $\langle (\delta\chi)^2 \rangle$  is determined by  $(V_0 + iW_0)^2$ . If the dynamic polarization potential is contributed dominantly by the term  $\frac{i}{2} \langle (\delta\chi)^2 \rangle$ , its sign follows  $-i(V_0 + iW_0)^2$ , so the real and imaginary parts of the dynamic polarization potential have the same sign as  $V_0W_0$  and  $W_0^2 - V_0^2$ , respectively.

We compare in Fig. 6 the  $^6\text{He}+^{12}\text{C}$  single-folding potential (dashed line) with the optical potential calculated from the eikonal approximation (solid line). The breakup process produces a repulsive surface effect on the real part of the optical potential and increases a strength of the imaginary part reflecting the loss of the flux due to the elastic breakup process. Dash-dotted and dotted lines in the figure denote the optical potential and the single-folding potential for  $^4\text{He}+^{12}\text{C}$  scattering calculated at the same energy of 40 MeV/nucleon. The breakup effect does not practically change the real part of the potential but moderately increases the strength of the imaginary part for the  $^4\text{He}+^{12}\text{C}$  case. The effect becomes very significant for the  $^6\text{He}+^{12}\text{C}$  case. In particular the imaginary part of the  $^6\text{He}-^{12}\text{C}$  optical

potential becomes much longer-ranged and almost twice stronger than that of the  ${}^4\text{He}-{}^{12}\text{C}$  optical potential.

Next we study the energy dependence of the breakup effect. Figure 7 shows calculated  ${}^6\text{He}+{}^{12}\text{C}$  elastic differential cross sections at different energies from 70 MeV/nucleon to 800 MeV/nucleon. We used the  $p-{}^{12}\text{C}$  global optical potential [31]. The energy dependence of this potential is as follows: The real part at the center alters as  $-32.3, -11.7, 16.2$  MeV, for 70, 200, 800 MeV/nucleon, respectively, while the imaginary part as  $-0.9, -12.0, -87.2$  MeV. Solid line in Fig. 7 denotes the eikonal calculation, while dashed line the folding-model calculation. Figure 8 compares the real and imaginary parts of the  ${}^6\text{He}-{}^{12}\text{C}$  optical potential  $U(R)$  determined from the phase-shift function with those of the single-folding potential  $U_f(R)$ . The real part of the folding potential becomes shallower as the energy increases and turns out to be repulsive at 800 MeV/nucleon, whereas the imaginary part of the folding potential becomes deeper with the energy increasing. At 70 MeV/nucleon both of the real and imaginary parts of the  $p-{}^{12}\text{C}$  global optical potential is negative and  $V_0^2 > W_0^2$ , so the first term of the dynamic polarization potential has positive real and negative imaginary parts, respectively. This explains why the optical potential is less attractive and more absorptive than the single-folding potential at this energy. At 800 MeV/nucleon the global potential has positive real and negative imaginary parts with  $W_0^2 > V_0^2$ , so the first term of the dynamic polarization potential has a negative sign for the real part and a positive sign for the imaginary part, which also explains the change of the optical potential from the single-folding potential at this energy. The magnitude of the dynamic polarization potential at 800 MeV/nucleon is quite big: Quite large, negative imaginary potential of the folding potential is dramatically reduced to  $-49.3$  MeV at the center.

## V. SUMMARY

With the Monte Carlo integration we evaluated the scattering amplitude of the Glauber model without any *ad hoc* approximation. The advantage of this approach is that one can use accurate, sophisticated wave functions of colliding nuclei.

We studied the elastic scattering of  ${}^6\text{He}+{}^{12}\text{C}$  at 40 MeV/nucleon in order to see the breakup effect of a weakly bound halo nucleus  ${}^6\text{He}$ . Comparing to the new  ${}^6\text{He}+{}^{12}\text{C}$  data which cover larger angles than the previous data, we found that the complete Galuber amplitude with use of a realistic VMC wave function for  ${}^6\text{He}$  reproduced experiment only at small angles but beyond the first minimum gave too small differential cross sections. Calculating the phase-shift function with a nucleon- ${}^{12}\text{C}$  optical potential, we were able to reproduce the experimental data reasonably well. In this calculation the breakup effect of  ${}^6\text{He}$  was taken into account in the eikonal approximation.

Through the calculated phase-shift function we constructed the  ${}^6\text{He}-{}^{12}\text{C}$  optical potential which contains the dynamic polarization potential due to the breakup effect of  ${}^6\text{He}$ . This optical potential has a longer range and a deeper depth than that of the  ${}^4\text{He}-{}^{12}\text{C}$  optical potential. The difference between the two potentials appears more strongly in the imaginary part. We studied the elastic scattering of  ${}^6\text{He}+{}^{12}\text{C}$  at different energies and discussed the energy dependence of the dynamic polarization potential from 40 to 800 MeV/nucleon. The effect of the breakup is so strong that e.g., the imaginary part of the dynamic polarization

potential renders the central depth of the folding potential ( $-314.1$  MeV) considerably shallow ( $-49.3$  MeV).

The approach presented here has the strength that it makes it possible to directly relate cross sections to relevant wave functions. We thus hope that the new radioactive beam facilities will produce experimental data covering larger angles.

## VI. ACKNOWLEDGEMENTS

The authors thank K. Varga, V. Lapoux, B. C. Clark, N. Orr and J. Y. Hostachy for useful communications. One of the authors (B. A-I.) is supported by a JSPS Postdoctoral Fellowship for Foreign Researchers (No. P03023). This work was in part supported by a Grant-in-Aid for Scientific Research (No. 14540249) of the Ministry of Education, Science, Sports and Culture (Japan).

## TABLES

TABLE I. Reaction cross sections in mb for  $p+^{12}\text{C}$  and  ${}^6\text{He}+^{12}\text{C}$  reactions predicted by different  $p-^{12}\text{C}$  optical potentials.

Optical potential	$p+^{12}\text{C}$	${}^6\text{He}+^{12}\text{C}$
Fannon <i>et al.</i> [22]	380	1193
Becchetti and Greenlees [23]	377	1147
Rapaport [24]	396	1139

The experimental  $p+^{12}\text{C}$  reaction cross section is  $371 \pm 9$  mb [27].

## FIGURES

FIG. 1. Elastic differential cross sections in Rutherford ratio for  ${}^6\text{He}+{}^{12}\text{C}$  scattering at 40 MeV/nucleon. Solid line is the cross section calculated with a single-folding model in which the  $p-{}^{12}\text{C}$  optical potential [24] is folded with the VMC density [13]. Dotted and dashed lines are full Glauber-model calculations which employ the sets of  $\Gamma_{NN}$  parameters as explained in text. The data are taken from Refs. [1,2].

FIG. 2. Elastic differential cross sections in Rutherford ratio for  ${}^4\text{He}+{}^{12}\text{C}$  scattering at 40 MeV/nucleon. The VMC wave function for  ${}^4\text{He}$  [13] is used. Solid, dash-dotted and dashed lines denote the results with three different  $p-{}^{12}\text{C}$  optical potentials [22–24], respectively. Dotted line is the cross section calculated by using the single harmonic-oscillator shell-model wave function for  ${}^4\text{He}$  and the potential of Ref. [22] but by ignoring the c.m. correlation as explained in text. The data are taken from Refs. [26].

FIG. 3. Elastic differential cross sections in Rutherford ratio calculated in the eikonal approximation for  ${}^6\text{He}+{}^{12}\text{C}$  scattering at 40 MeV/nucleon. The VMC wave function for  ${}^6\text{He}$  [13] is used. Dotted, dashed and solid lines denote the results with three different  $p-{}^{12}\text{C}$  optical potentials [22–24], respectively.

FIG. 4. The same as in Fig. 3 but by a partial-wave expansion for the scattering amplitude.

FIG. 5. The same as in Fig. 3 but by the few-body Glauber model. See text for the three-body wave function and the  $\alpha-{}^{12}\text{C}$  potential employed in the calculation.

FIG. 6. Real and imaginary parts of the  ${}^6\text{He}-{}^{12}\text{C}$  optical potential at 40 MeV/nucleon. Solid line includes the breakup effect of  ${}^6\text{He}$ , while dashed line is the single-folding potential. The difference of the two potentials is the dynamic polarization potential. The  $p-{}^{12}\text{C}$  optical potential [24] is used. Dash-dotted and dotted lines denote the optical and single-folding potentials for  ${}^4\text{He}-{}^{12}\text{C}$  at 40 MeV/nucleon, respectively. The VMC wave functions [13] are used for both  ${}^6\text{He}$  and  ${}^4\text{He}$ .

FIG. 7. Elastic differential cross sections in Rutherford ratio for  ${}^6\text{He}+{}^{12}\text{C}$  scattering calculated at different energies. The  $p-{}^{12}\text{C}$  optical potential is taken from Ref. [31]. The VMC wave function [13] is used for  ${}^6\text{He}$ . Solid line is the eikonal calculation, while dashed line is the single-folding model calculation.

FIG. 8. Real (a) and imaginary (b) parts of the  ${}^6\text{He}-{}^{12}\text{C}$  optical potential at different energies. Solid line includes the breakup effect of  ${}^6\text{He}$ , while dashed line is the single-folding potential. The  $p-{}^{12}\text{C}$  optical potential is taken from Ref. [31]. The VMC wave function [13] is used for  ${}^6\text{He}$ .

## REFERENCES

- [1] V. Lapoux *et al.*, Phys. Rev. C **66** (2002) 034608.
- [2] J. S. Al-Khalili *et al.*, Phys. Lett. B **378** (1996) 45.
- [3] see, for example, Y. Suzuki, R. G. Lovas, K. Yabana and K. Varga, *Structure and Reactions of Light Exotic Nuclei* (Taylor & Francis, London, 2003).
- [4] K. Arai, Y. Suzuki and R. G. Lovas, Phys. Rev. C **59** (1999) 1432.
- [5] G. R. Satchler and W. G. Love, Phys. Rep. **55** (1979) 184.
- [6] Y. Sakuragi, M. Yahiro and M. Kamimura, Prog. Theor. Phys. Suppl. No. 89 (1986) 136.
- [7] K. Yabana, Y. Ogawa and Y. Suzuki, Phys. Rev. C **45** (1992) 2909.
- [8] J. S. Al-Khalili, I. J. Thompson and J. A. Tostevin, Nucl. Phys. A **581** (1995) 331.
- [9] G. F. Bertsch, K. Hencken and H. Esbensen, Phys. Rev. C **57** (1998) 1366.
- [10] A. Bonaccorso and D. M. Brink, Phys. Rev. C **58** (1998) 2864.
- [11] R. J. Glauber, in *Lectures on Theoretical Physics*, edited by W. E. Brittin and L. C. Dunham (Interscience, New York, 1959), Vol.1, p.315.
- [12] B. Abu-Ibrahim and Y. Suzuki, Nucl. Phys. A **706** (2002) 111.
- [13] B. S. Pudliner, V. R. Pandharipande, J. Carlson, S. C. Pieper and R. B. Wiringa, Phys. Rev. C **56** (1997) 1720.
- [14] J. S. Al-Khalili, J. A. Tostevin and J. M. Brooke, Phys. Rev. C **55** (1997) R1018; J. M. Brooke, J. S. Al-Khalili and J. A. Tostevin, Phys. Rev. C **59** (1999) 1560.
- [15] K. Varga, S. C. Pieper, Y. Suzuki and R. B. Wiringa, Phys. Rev. C **66** (2002) 034611.
- [16] R. B. Wiringa, V. G. J. Stocks and R. Schiavilla, Phys. Rev. C **51** (1995) 38.
- [17] S. C. Pieper, V. R. Pandharipande, R. B. Wiringa and J. Carlson, Phys. Rev. C **64** (2001) 014001.
- [18] D. R. Thompson, M. LeMere and Y. C. Tang, Nucl. Phys. A **286** (1977) 53.
- [19] S. M. Lenzi, A. Vitturi and F. Zurdi, Phys. Rev. C **40** (1989) 2114.
- [20] J. Y. Hostachy, Thèse d'Etat, I.S.N. 87-65, Université de Grenoble, unpublished.
- [21] B. Abu-Ibrahim and Y. Suzuki, Phys. Rev. C **61** (2000) 051601(R); *ibid.* **62** (2000) 034608.
- [22] J. A. Fannon, E. J. Burge, D. A. Smith and N. K. Ganguly, Nucl. Phys. A **97** (1967) 263.
- [23] F. D. Becchetti and G. W. Greenlees, Phys. Rev. **182** (1969) 1190.
- [24] J. Rapaport, Phys. Rep. **87** (1982) 25.
- [25] L. N. Blumberg, E. E. Gross, A. van der Woude, A. Zucker and R. H. Bassel, Phys. Rev. **147** (1966) 812.
- [26] B. Tatischeff and I. Brissaud, Nucl. Phys. A **155** (1970) 89.
- [27] R. F. Carlson, Atomic Data and Nuclear Data tables **63** (1996) 93.
- [28] W. Czyz and L. C. Maximon, Ann. Phys. (N.Y.) **52** (1969) 59.
- [29] V. Franco and G. K. Varma, Phys. Rev. C **18** (1978) 349.
- [30] Y. Suzuki, T. Kido, Y. Ogawa, K. Yabana and D. Baye, Nucl. Phys. A **567** (1994) 957.
- [31] E. D. Cooper, S. Hama, B. C. Clark and R. L. Mercer, Phys. Rev. C **47** (1993) 297.

Fig. (2)

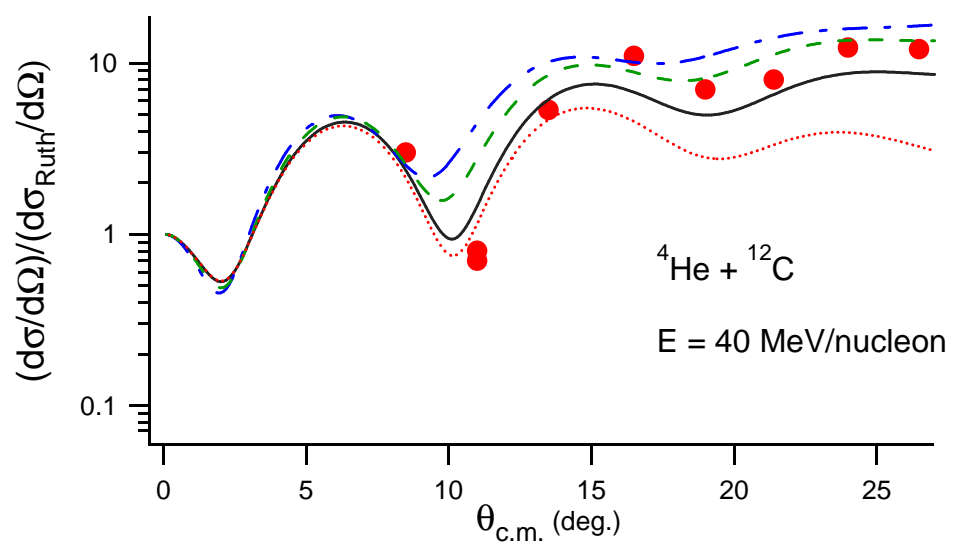


Fig. (7)

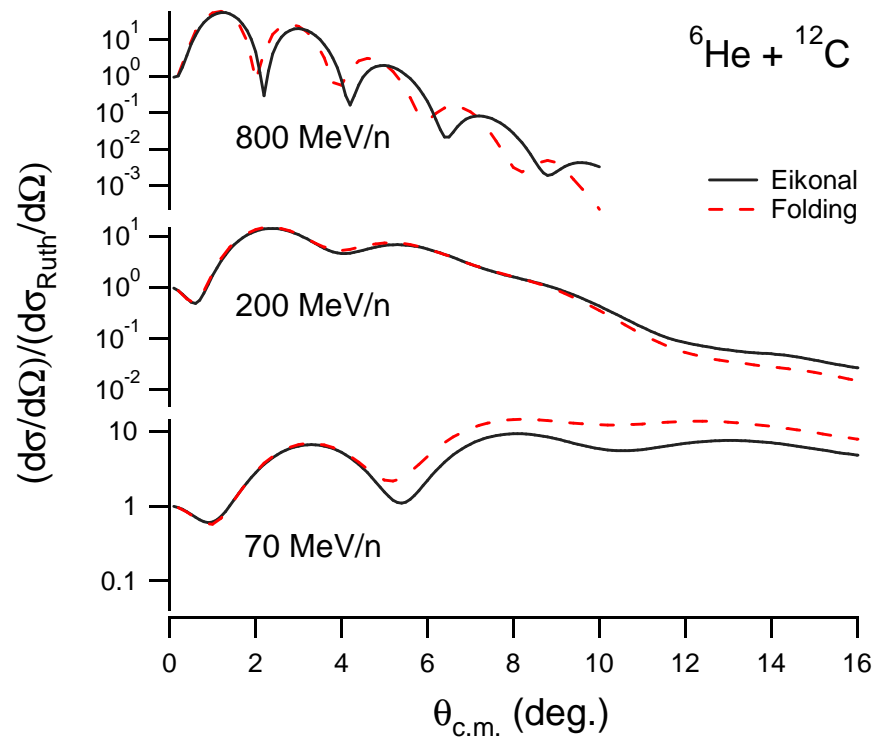


Fig. (5)

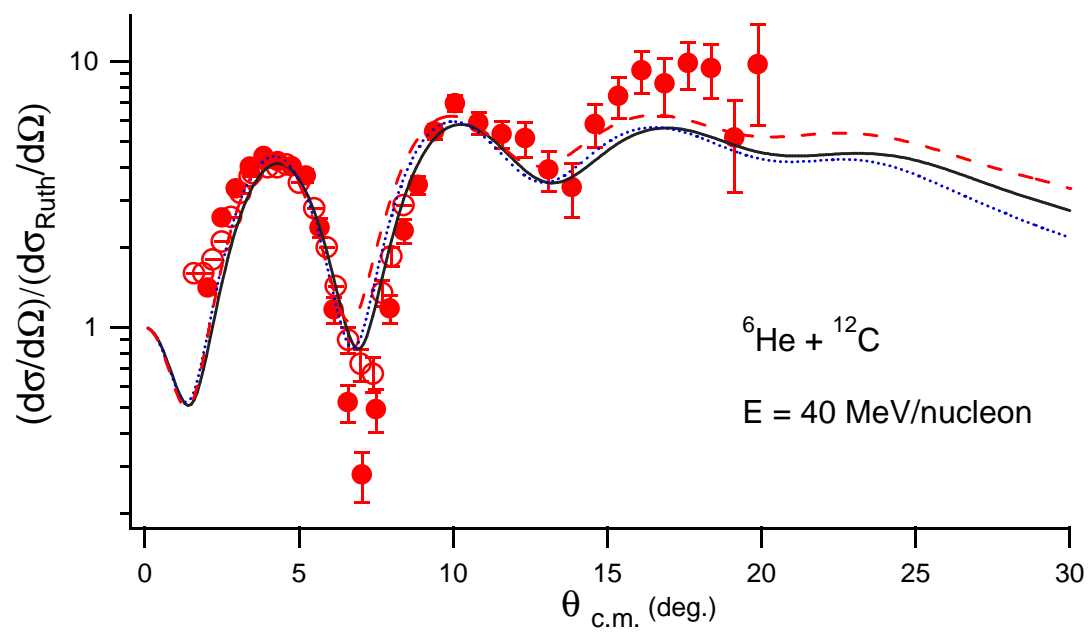


Fig. (1)

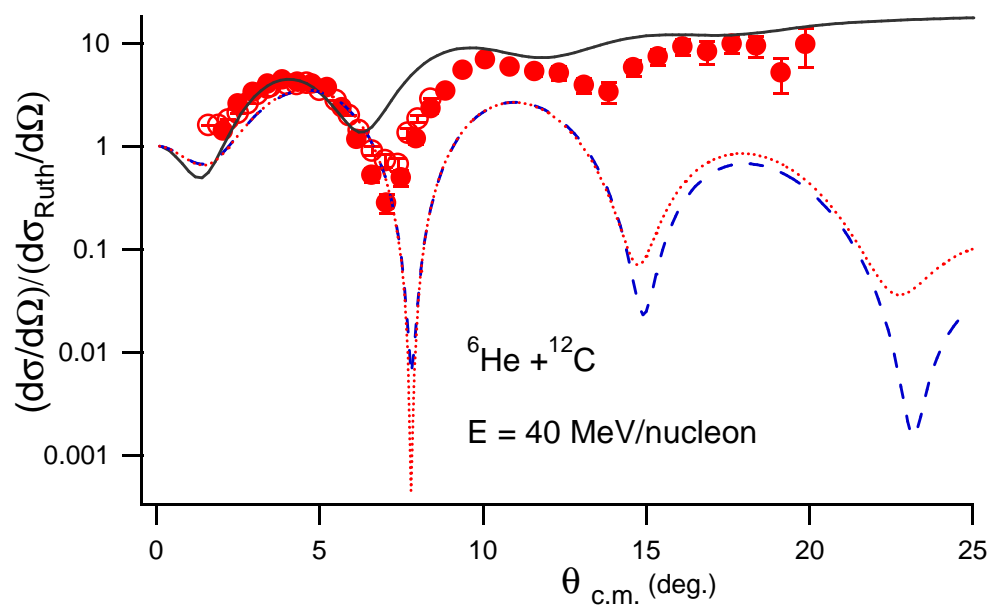


Fig. (8)

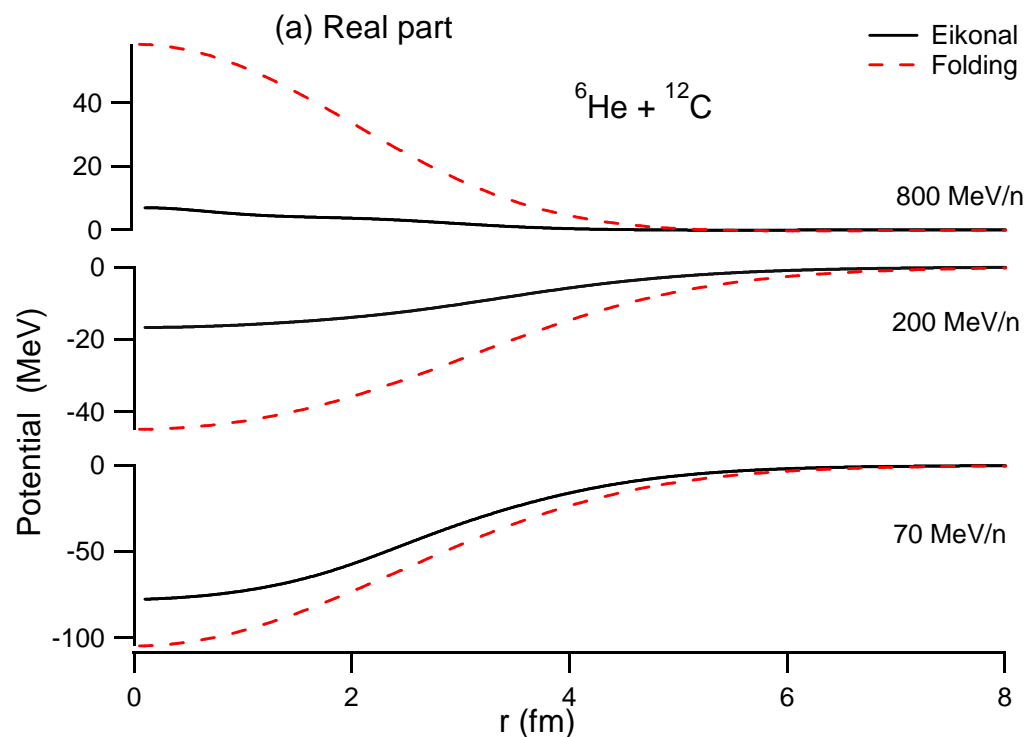


Fig. (8)

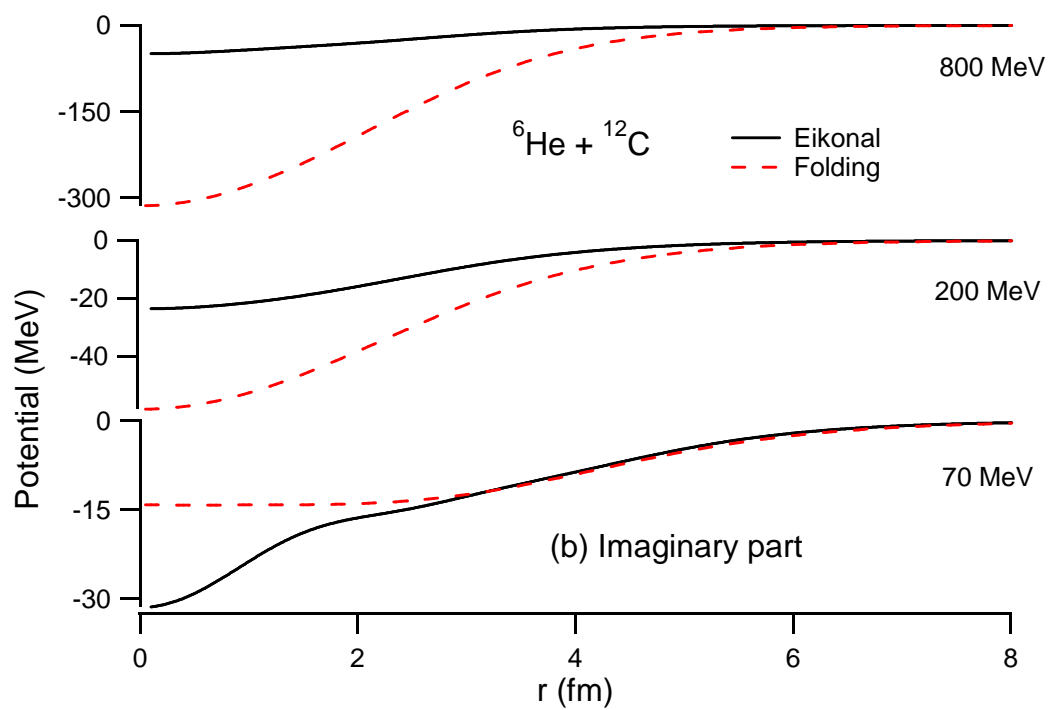


Fig. (6)

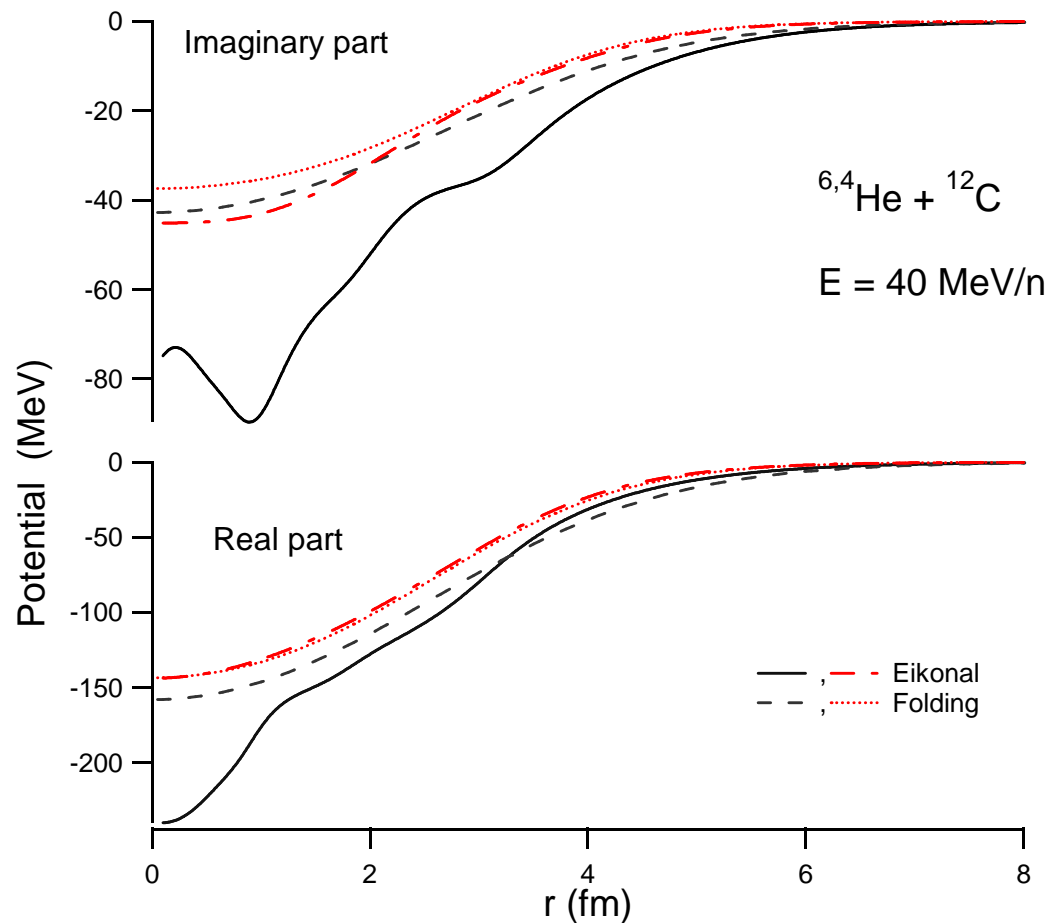


Fig. (4)

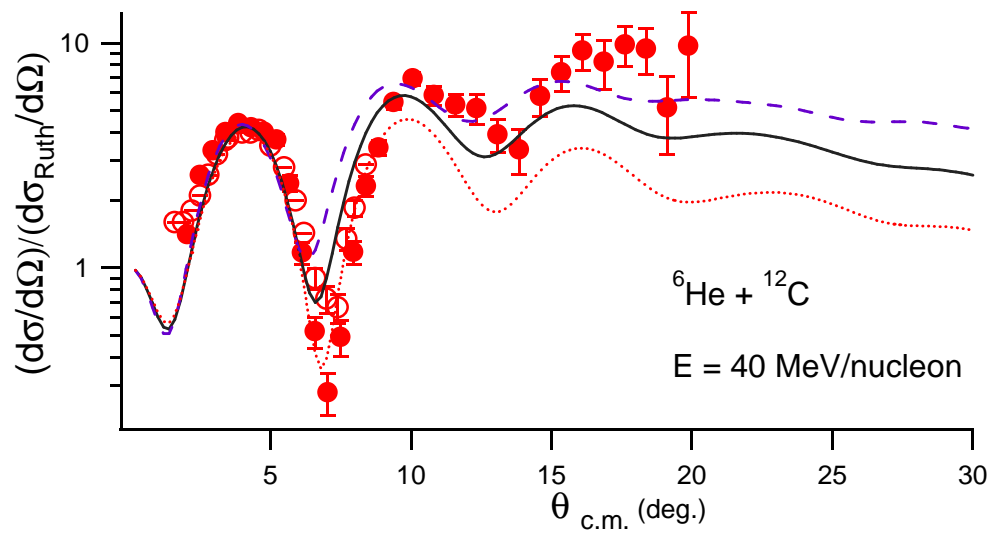


Fig. (3)

